

RESEARCH ARTICLE

10.1002/2017MS000965

Colliding Modons: A Nonlinear Test for the Evaluation of Global Dynamical Cores

Shian-Jiann Lin¹ , Lucas Harris¹ , Xi Chen² , Weiye Yao², and Junyi Chai²

¹NOAA/Geophysical Fluid Dynamics Laboratory, Princeton University, Princeton, NJ, USA, ²Program in Atmospheric and Oceanic Sciences, Princeton University, Princeton, NJ, USA

Key Points:

- A new test of the horizontal nonlinear vorticity dynamics in a dynamical core is presented, applicable to both shallow-water and 3-D cores
- This “modon” test is easy-to-setup and can create a perpetual cycle of vortex pairs colliding, exchanging, and reforming
- The test isolates the horizontal discretization, and the results are sensitive to the horizontal dissipation in a core

Correspondence to:

S.-J. Lin,
shian-jiann.lin@noaa.gov

Citation:

Lin, S.-J., Harris, L., Chen, X., Yao, W. & Chai, J. (2017). Colliding modons: A nonlinear test for the evaluation of global dynamical cores. *Journal of Advances in Modeling Earth Systems*, 9, 2483–2492. <https://doi.org/10.1002/2017MS000965>

Received 7 MAR 2017

Accepted 15 SEP 2017

Accepted article online 21 SEP 2017

Published online 10 NOV 2017

© 2017. The Authors.

This is an open access article under the terms of the Creative Commons Attribution-NonCommercial-NoDerivs License, which permits use and distribution in any medium, provided the original work is properly cited, the use is non-commercial and no modifications or adaptations are made.

Abstract The modon, a pair of counter-rotating vortices propelling one another along a straight line, is an idealization of some observed large-scale and small-scale atmospheric and oceanic processes (e.g., twin cyclones), providing a challenging nonlinear test for fluid-dynamics solvers (known as “dynamical cores”). We present an easy-to-setup test of colliding modons suitable for both shallow-water and three-dimensional dynamical cores on the sphere. Two pairs of idealized modons are configured to collide, exchange vortices, and depart in opposite directions, repeating indefinitely in the absence of ambient rotation. This test is applicable to both hydrostatic and nonhydrostatic dynamical cores and is particularly challenging for refined grids on the sphere, regardless of solution methodology, or vertical coordinate. We applied this test to three popular dynamical cores, used by three different general circulation models: the Spectral-Element (SE) core of the Community Atmosphere Model, the Geophysical Fluid Dynamics Laboratory (GFDL) spectral core, and the GFDL Finite-Volume Cubed-Sphere dynamical core (FV³). Tests with a locally refined grid and nonhydrostatic dynamics were also performed with FV³. All cores tested were able to capture the propagation, collision, and exchange of the modons, albeit the rate at which the modon was diffused varied between the three cores and showed a strong dependence on the strength of hyperdiffusion.

1. Introduction

Idealized testing of Atmospheric General Circulation Model (AGCM) components is an essential part of weather-climate model development and validation, as it can reveal the capabilities or expose potential flaws of the numerical design. A number of tests have been proposed for atmospheric dynamical cores (Held & Suarez, 1994; Jablonowski & Williamson, 2006; Reed & Jablonowski, 2012; Robert, 1993; Schär et al., 2002; Straka et al., 1993; Williamson et al., 1992), results for a number of which can be found at <http://www.cgd.ucar.edu/cms/pel/colloquium.html>, https://earthsystemcog.org/projects/dcmip-2012/Test_Cases/results_by_model, and <https://www.earthsystemcog.org/projects/dcmip-2016>; see Ullrich et al. (2012) for more information. These tests provide useful qualitative information, although few have exact solutions, and in many cases it is difficult if not impossible to know the “correct” solution, necessitating subjective judgements by developers and evaluators. Some of these tests are designed for Cartesian-coordinate, limited-area models, with grid spacings of a few kilometers or finer, and may only be extendable to the sphere by performing special initialization methods or by artificially reducing the radius of the sphere (the small-earth approximation) to make it computationally feasible. Many tests intended for spherical geometry were designed only for shallow-water flows and are difficult to extend to three dimensions. Finally, some of these tests focus mainly on linear and/or divergent motions, despite the primacy of the strongly rotational and nonlinear nature of severe weather events, such as hurricanes, tornadoes, extratropical cyclones, and in the eddies vital to atmosphere-ocean interaction. The rotational component of atmospheric flows is vital to the fidelity and the success of the simulations. Less recognized is its impact to the air-sea coupling: the dynamical impact of the atmosphere to the ocean is mainly through the curl of the surface wind stress, which is exerted by the rotational component of the atmospheric motion. Models designed for regional cloud-scale simulation tend to emphasize the importance of the divergent component, rather than the rotational component. Idealized tests with nonlinear rotational flows may expose design flaws in such models.

A fascinating dynamical phenomenon occurs when two counter-rotating fluid vortices interact with one another. Instead of merging or revolving around each other, they instead mutually push one another in the same direction as if they were a single coherent feature in the fluid. This feature is most commonly called a

Table 1
Interface Pressures and Heights for the Five-Level Setup for a Stratified Model

z (km)	0	2	4	6	8	10
p (hPa)	1000.0	796.43	634.31	505.18	402.35	320.44
ak (hPa)	0.00	46.43	134.31	255.18	402.35	320.44
bk	1.00	0.75	0.50	0.25	0.00	0.00

Note. Geometric heights are given for a 300 K isothermal atmosphere. A reference set of hybrid coordinate coefficients is provided.

“modon” (Flierl, 1987; Muraki & Snyder, 2007; Tribbia, 1984) in atmospheric science. Applied mathematicians call them “solitons,” owing to both their nonlinearity and the fact that they can steadily propagate in a straight line as if they were solitary waves (Ingersoll, 1973). More rarely, some physicists refer to them as “quarks,” since the vortices cannot exist in isolation, and if disturbed or separated the feature quickly breaks down. Exact solutions for counter-rotating vortices have long been known (Batchelor, 1967; Lamb, 1932, section 155) for laboratory-scale flows, and extensions to the sphere have shown great utility for studying many geophysical phenomena: cold-core oceanic rings (Flierl, 1979), atmospheric blocking (Butchart et al., 1989; McWilliams, 1980), the Rex (1950) block, often described as a modon; spontaneous imbalance (Vanneste, 2013); and localized atmospheric jets (Muraki & Snyder, 2007).

We present a variant of the modon solution as a simple (to setup) yet challenging (to perform) test case for dynamical cores. This test is initialized with a localized zonal jet streak (akin to a westerly wind burst within the context of the Madden-Julian Oscillation (MJO)) in a nonrotating atmosphere without attempting to satisfy the balance constraints in either the meridional wind, temperature, or in the pressure field. The model is initialized with two opposing modons along the equator at antipodal points on the sphere, with one propagating eastward and the other westward. Without the planetary rotation, each of the modons quickly adjusts to a cyclostrophically balanced state, developing the quadrupole meridional wind pattern and pair of cyclones characteristic of a balanced modon. The two modons then propagate toward each other; upon colliding, the modons do not merge, but instead the positive/negative vortices are exchanged, forming two new modons which then propagate poleward away from each other, with their original structure intact. Upon crossing the pole and returning to the equator, the modons collide again, exchanging vortices and again moving away from each other along the equator. This periodic process can, in principle, repeat indefinitely as long as the modons are not diffused (numerically) and if there are no other numerical errors which cause the modon to break by disrupting the symmetry of the vortices in the modon.

By leaving the initial state unbalanced and without the Coriolis force, the test is straightforward to set up, and generates a nearly perpetual cycle of collision and exchange, if the numerical errors are small. The initial adjustment process and the nonlinear vortex dynamics in this test make it a

valuable test of the horizontal discretization of the dynamical core. In particular, spurious vorticity generation may disrupt the vortex symmetry sufficiently to cause the modon to break. A model with spurious vorticity generation revealed by this test could potentially possess similar problems in a full-physics model, with attendant issues in weather and climate simulations such as in the propagation of tropical cyclones.

This colliding modons test case appears to be ideal for a shallow-water solver. However, to evaluate the ability of a three-dimensional solver’s ability to handle nonlinear rotational flows and the potential effects of the vertical coordinate or the nonhydrostatic solver, we therefore also present a vertically homogeneous, isothermal variation of the test case. This test can be applied to both hydrostatic and nonhydrostatic solvers, regardless of the choice of vertical coordinate, as long as the shallow-atmosphere assumption is made. We present results from several different dynamical cores: shallow-water and hydrostatic simulations using the GFDL spectral core (Held & Suarez, 1994), hydrostatic simulations using the spectral-element core of the Community Atmosphere Model (CAM-SE) (Taylor & Fournier, 2010), and shallow-water and nonhydrostatic simulations using the GFDL finite-volume cubed-sphere dynamical core (FV³) (Harris & Lin, 2013; Putman & Lin, 2007). The test design and evaluation are robust enough to be applicable to a wide range of solver types, numerical methods, and dynamical core and grid configurations. In particular, we do not prescribe a certain

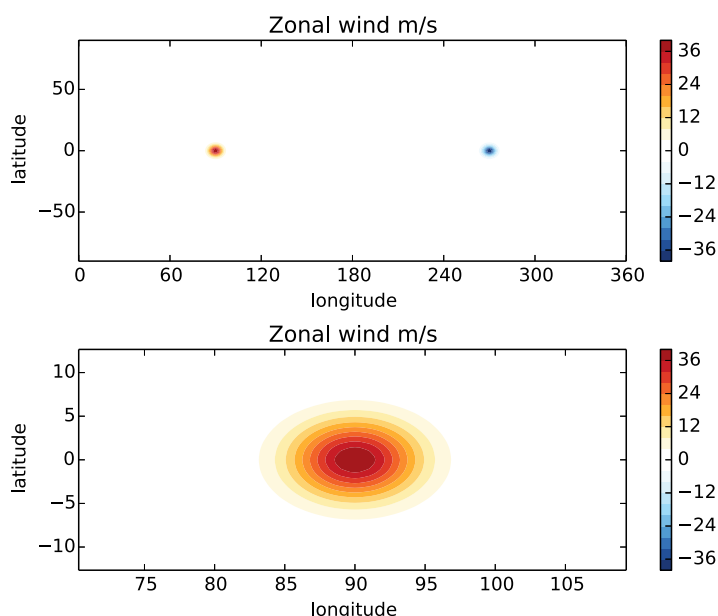


Figure 1. Initial zonal wind field for all model levels. (top) A positive (westerly wind) Gaussian wind at 90 degrees east and a negative (easterly wind) Gaussian wind at 90 degrees west (i.e., 270 degrees east). (bottom) A zoom-in view of the positive zonal wind perturbation at 90 degrees east.

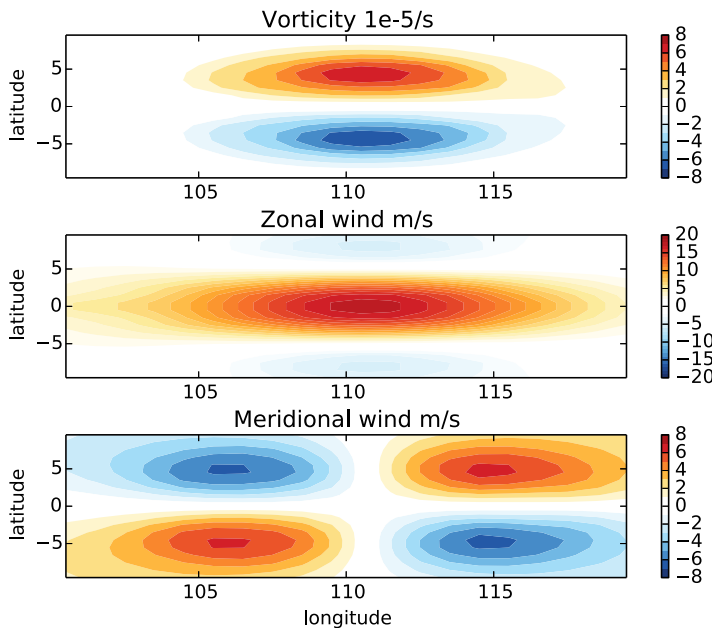


Figure 2. Lower-most model level structure of the eastward moving modon on day 5, after adjustment, in C192 (or equivalently 50 km) resolution shallow-water FV³. (top) Relative vorticity showing the two counter-rotating vortices. (middle) Zonal wind showing the westerly jet. (bottom) Meridional wind showing the quadrupole pattern.

amount or type of diffusion; our only recommendation is that modelers use the same type and same order of magnitude of artificial diffusion as would be used in a full-physics simulation, such as a climate model or weather-prediction system.

The primary goal of the test is to be able to maintain the symmetric modon pattern as long as possible, and to demonstrate that the dynamical core produces a minimum of nonsymmetric noise that can disturb the symmetry and cause the modon to break. This test procedure is analogous to that of the Rossby-Haurwitz wave, Case 6 in Williamson et al. (1992), which tests how long a dynamical core can maintain the symmetric global wave pattern. Further evaluation of the test can be done by computing the amplitude of the modons and the form of the equilibrated modons.

Section 2 provides a comprehensive test description, including the analytical form of the initial condition and the extension to three-dimensional stratified flows. Section 3 provides the test result from different dynamical cores. A final discussion is provided in section 4.

2. Test Description

2.1. Specification of the Modons

In a shallow-water model, the initial flow depth is set to a uniform 10 km. In a three-dimensional model, for simplicity, the atmosphere is assumed to be isothermal at 300 K with uniform initial surface pressure of 1,000 hPa and a model top at 10 km; pressure fields can

be derived from hydrostatic balance (given height fields, see Table 1). The user is free to choose the vertical coordinate and total number of layers in such a stratified configuration. As it should become clear, the vertical resolution bears no consequence to the test results. In our stratified-model simulations, we chose, for convenience, a five-level setup defined in Table 1, with each layer 2 km thick. We have also validated this test with an extremely fine vertical resolution of 55 layers in CAM-SE. Both FV³ and CAM-SE use the Lagrangian vertical coordinate (Lin, 2004) with a hybrid-pressure Eulerian reference coordinate, but the same vertical levels can be used in a height-coordinate model without modification.

Unlike other modon tests (e.g., Muraki & Snyder, 2007; Snyder et al., 2007; Tribbia, 1984), this test specifies no planetary rotation. While the Coriolis force is important in many atmospheric processes, we have decided to turn it off to simplify the test configuration, to allow the modons to propagate initially westward and eastward, and to avoid the need to specify a complex geostrophically balanced initial state. Turning off the ambient rotation is common for idealized testing and intercomparison (e.g., Reed et al., 2015; Schär et al., 2002).

A single modon is initially defined by the zonal wind perturbation:

$$M_i = U_0 \exp \left[- (r_i / r_0)^2 \right]. \quad (1)$$

The initial state consists of two oppositely signed zonal wind perturbations:

$$u'(\lambda, \theta) = M_1 - M_2, \quad (2)$$

where $U_0 = 40$ m/s, $r_0 = 500$ km, r_1 and r_2 are the great-circle distance from the center of each modon, and (λ, θ) are the longitude and latitude, respectively. The modons are initially centered at $(\lambda_1, \theta_1) = (\pi/2, 0)$, $(\lambda_2, \theta_2) = (3\pi/2, 0)$. The full initial flows, both the basic state and the modons, are vertically uniform and thereby the flow is initially barotropic. Unlike Muraki and Snyder (2007), the perturbation in zonal wind is a smooth Gaussian, and so less prone to create

Table 2
A Summary of the Explicit Diffusion Mechanisms in the Three Dynamical Cores Presented in this Paper

CAM-SE	DTIME	1,200
	se_nsplit	3
	rsplit	3
	qsplitt	1
	tstep_type	5
	nu_div	2e13
	nu	5e13
	nu_top	0
	nu_p	2e13
GFDL spectral	Hyperviscosity damping time scale on highest wave number	0.1 d
	GFDL FV ³	Dimensionless divergence damping coefficient

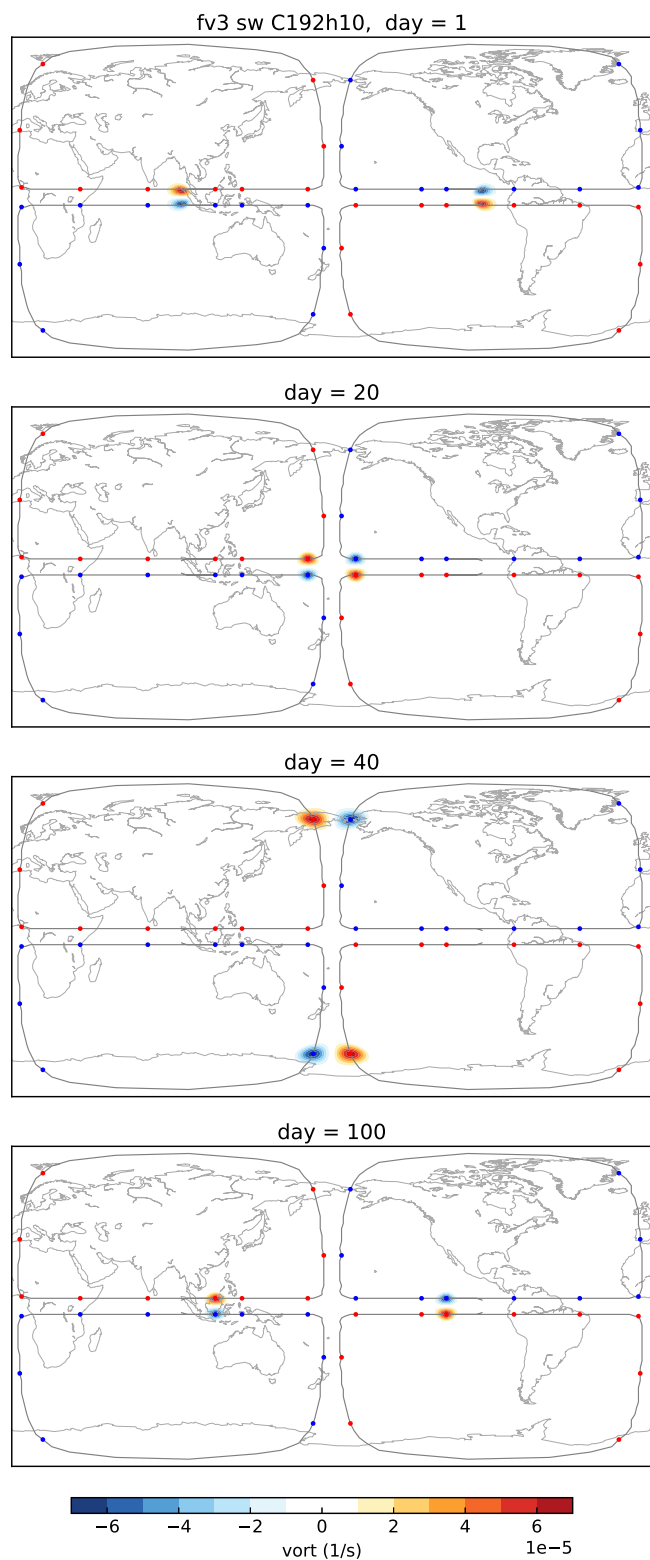


Figure 3. Vorticity (colored shading) from C192 shallow-water FV³ simulations at days 1, 20, 40, and 100 (top to bottom). The trajectories of the vortices are given by the gray curve, with colored dots showing the location of the vortices at 10 day intervals. Coastlines are shown for reference purposes only.

Gibbs oscillations in spectral models. The initial zonal wind is depicted in Figure 1. The background state is at rest and horizontally homogeneous. The initial state has no vertical motion, and the simulations have no topography or moisture.

2.2. Basic Characteristics of the Modons

The modons travel at an MJO-like speed (6–7 m/s) along the equator until they collide. After the initial rapid cyclostrophic adjustment, two sets of twin-vortex pairs form and propagate steadily toward each other. Since the modons are initially symmetric and there is no planetary rotation, the flow is symmetric about both $\theta = 0$ (equator) and $\lambda = \pi$. The structure of the eastward moving modon at day 5 after the initial adjustment is shown in Figure 2. The left (western) modon pair is created by the westerly wind burst, with a positive vortex in the Northern Hemisphere and negative vortex in the Southern Hemisphere, and traveling toward the east. The right (eastern) modon pair is created by the easterly windburst and creates a similar vortex pair, but with the signs of the vortices reversed and traveling toward the west. Although we show the lowest model level in this and all other figures, in the stratified and nonhydrostatic simulations, the solutions are visually the same on each level.

Although external gravity waves are excited by the initial unbalanced perturbations, the gravity waves rapidly decay after a few days due to numerical dissipation, either implicit or explicit. This wave radiation is common to other soliton tests (cf., Snyder et al., 2007). We find that this external gravity wave mode has a 1 day period in all three cores tested, as seen in the surface pressure field. The structure of the modons are not affected by these external modes, which will not be considered further.

We also found that the flow height does not affect the propagation of the modons. The gravity wave speed does change with flow height, but the amplitude of the gravity wave is much smaller than that of the modons. Tests using a 5 km flow height in the shallow-water model are almost identical to the 10 km flow height runs.

The stratified-flow variant of this test case can be formulated in a pressure or height-based vertical coordinate model without modification. While our stratified tests use models with a constant pressure upper boundary, the test is applicable to solvers with a rigid lid at the upper boundary, as was done in many earlier modon tests. However, a wave-absorbing upper boundary condition (e.g., Rayleigh friction or a diffusive sponge layer) that increases in strength with height should not be applied, because that would create vertical asymmetries and potentially forcing vertical motion. In all cases, we strongly recommend that horizontal numerical dissipation, whether implicit or explicit, be used, and that any numerical dissipation be of the same type and order of magnitude as in a full-physics simulation, upper-boundary wave-absorbing layers excepted. Dissipation should be considered an intrinsic part of any numerical scheme (Scott et al., 2016), and it is important to perform the test with the same dissipation as would be used in a full-physics model. The following sections will reveal that the choice of numerical dissipation does affect the evolution of the modons.

3. Results From Three Dynamical Cores

We present results using three different dynamical cores: National Center for Atmospheric Research (NCAR) CAM-SE; the GFDL spectral dynamical core; and GFDL FV³. All dynamical cores are run with grid spacings (or the

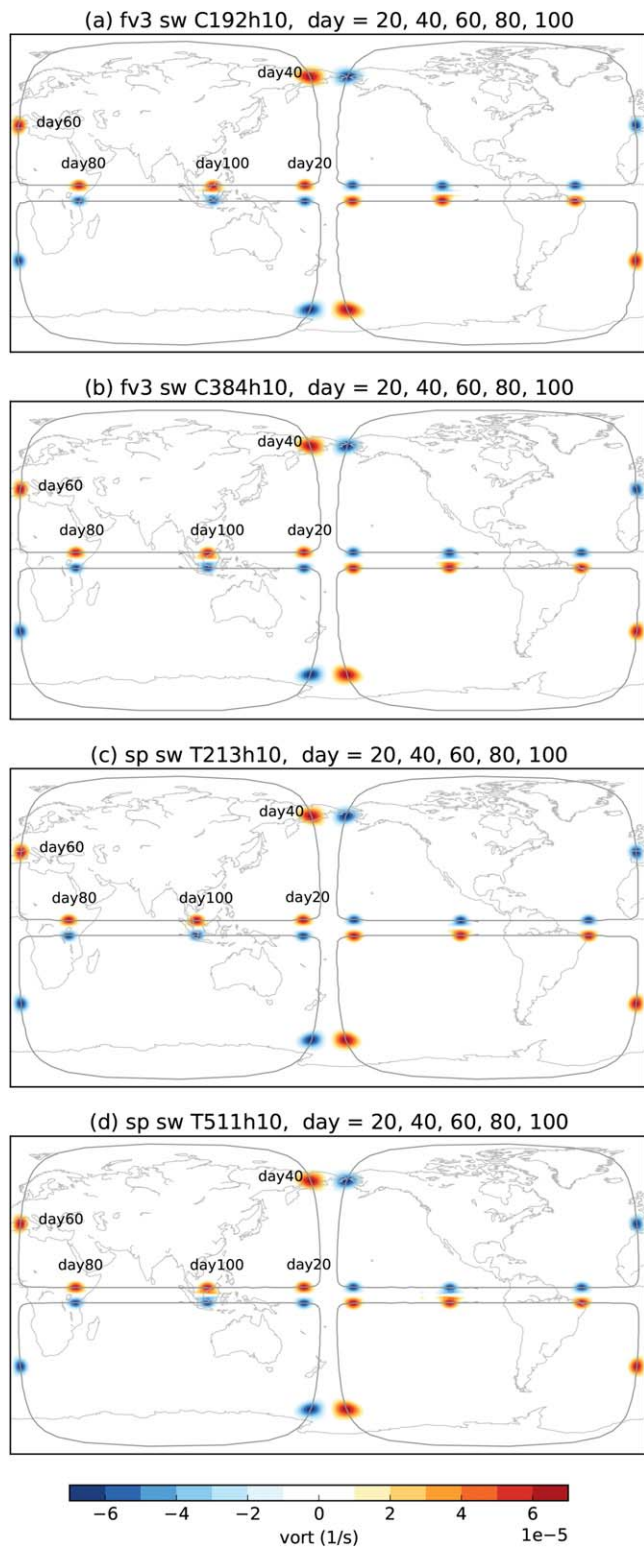


Figure 4. Vorticity fields of different shallow-water models at days 20, 40, 60, 80, and 100. (a) FV³ (C192, 50 km grid spacing, same result as in Figure 3); (b) FV³ C384; and the spectral-transform model at the resolutions; (c) T213 or 50 km resolution; and (d) T511 or 25 km resolution.

equivalent thereof) of roughly 0.5 degrees, with some additional using 0.25 degree resolution simulations; stratified-flow simulations use the five-level setup described earlier, with model top at 10 km (320.44 hPa using the initialization described in the previous section). We will also present results from the shallow-water configurations of the GFDL spectral core and of FV³. In addition, for FV³, we also present results from the nonhydrostatic solver and for a nonuniform stretched grid (Harris et al., 2016). It is found that while there are differences between each of the cores and the different solver configurations, the test case behaves similarly in all of the cores and configurations tested.

3.1. Description of the Dynamical Cores

The CAM-SE dynamical core solves the hydrostatic primitive equations using the continuous Galerkin spectral finite element method on a cubed-sphere grid (Taylor & Fournier, 2010). Each cube face consists of a number of elements inside of which the solution is integrated in spectral space of a given order of accuracy. The vertical discretization adopts the vertically Lagrangian approach (Lin, 2004). The configuration tested here uses a fourth-order solver with 60×60 elements on each cube face (ne60np4) and has 180 collocation points in each direction, equivalent to a 0.5 degree resolution. A fourth-order hyperviscosity with damping coefficient $2 \times 10^{13} \text{ m}^4 \text{ s}^{-1}$ is applied to divergence, tracers, and layer thickness, while a larger coefficient of $5 \times 10^{13} \text{ m}^4 \text{ s}^{-1}$ is applied to the other components of the flow. The core namelist parameters are given in Table 2, see an explanation of the parameters at http://www.cesm.ucar.edu/cgi-bin/eaton/namelist/nldef2html-cam5_3, and see Taylor and Fournier (2010) for further details of the implementation of the diffusion in CAM-SE.

The GFDL spectral dynamical core solves the hydrostatic primitive equations on a sphere with no bottom topography (Held & Suarez, 1994). The primitive equations are integrated with the spectral-transform method in the horizontal, and in stratified-flow simulations a centered finite-difference scheme is used in the vertical (using sigma coordinate). The only dissipative mechanism is an eighth-order hyperdiffusion imposed on the vorticity, divergence, and temperature fields, with a damping time scale of 0.1 day for the smallest waves, on the highest wave number. The hyperdiffusion coefficient is related to damping time scale by $\nu = \tau^{-1} (K(K+1))^{-4} R^8$, where τ is the damping time scale, K is the maximum resolved wave number, and R is the Earth's radius. The filter parameter in Robert-Asselin time filter is set to be 0.04. Dealiasing grid for the quadratic product is done in the standard manner by adding modes to the triangular truncation. More details on the diffusion in the spectral core are given in Scott and Polvani (2007). The spectral core is run with the T213 and T511 (triangular) truncations, equivalent to equatorial resolutions of 50 and 25 km, respectively.

The GFDL finite-volume cubed-sphere dynamical core (FV³) solves either the nonlinear shallow-water equations, the hydrostatic primitive equations, or the nonhydrostatic Euler equations, using the finite-volume method on the gnomonic cubed-sphere grid, as described by Putman and Lin (2007) and Harris and Lin (2013). The vector-invariant form of the shallow-water equations are solved following the Lin and Rood (1997) shallow-water algorithm in the horizontal on the dual Arakawa C and D-grid, with prognostic variables on the D-grid updated using a forward-backward time integration. The pressure gradient force is computed using the finite-volume algorithm of Lin (1997). Fluxes for mass, absolute vorticity, and kinetic energy are computed using a modification by Putman and Lin (2007) of the monotonic piecewise parabolic

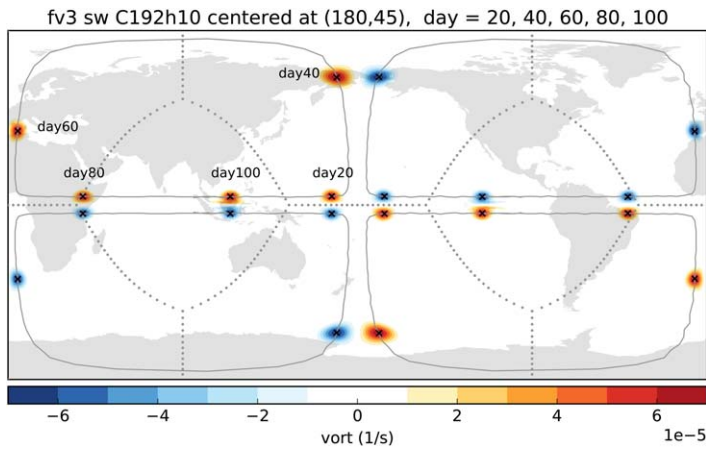


Figure 5. As in Figure 4a, but with the cubed-sphere grid rotated 45 degrees. The gray dots are the rotated-cubed-sphere tile interfaces. The markers (x) are the locations of the vortex from the run of the nonrotated grid.

method (Colella & Woodward, 1984). Unless otherwise stated, a sixth-order divergence damping with nondimensional coefficient $d_0=0.15$ is used to damp numerical noises near the grid-scale; this is an extension of the fourth-order divergence damping described in Zhao et al. (2012). No other explicit damping is specified. More information about the damping in FV³ is given at www.earthsystemcog.org/site_media/projects/dycore_test_group/20160127_Diffusion_operators.pdf. The rotational component of the flow is damped by the implicit diffusion associated with the piecewise parabolic method. The primitive-equation and nonhydrostatic solvers use a vertically Lagrangian mass-based coordinate in the vertical (Lin, 2004). The nonhydrostatic version, a nonessential component for this test, uses a more traditional semi-implicit solver for vertically propagating fast waves. A nonstaggered nonhydrostatic variation is described by Chen et al. (2013). Two uniform-resolution grids are presented: a C192 grid, with 192 grid cells across a cube face and an average grid-cell-width of 50 km, and a C384 grid, with 384 grid cells across a cube face and an average grid-cell-width of 25 km.

3.2. Shallow-Water Solutions

Figure 3 shows the vorticity field in the shallow-water FV³ with 50 km or C192 resolution. A 100 day simulation is presented, with gray curves showing the trajectories of the vortices. At day 1, the modon pairs have left their initial positions and started traveling toward each other along the equator, colliding and exchanging positive/negative vortices between days 20 and 30. By design, the modons travel at an approximately

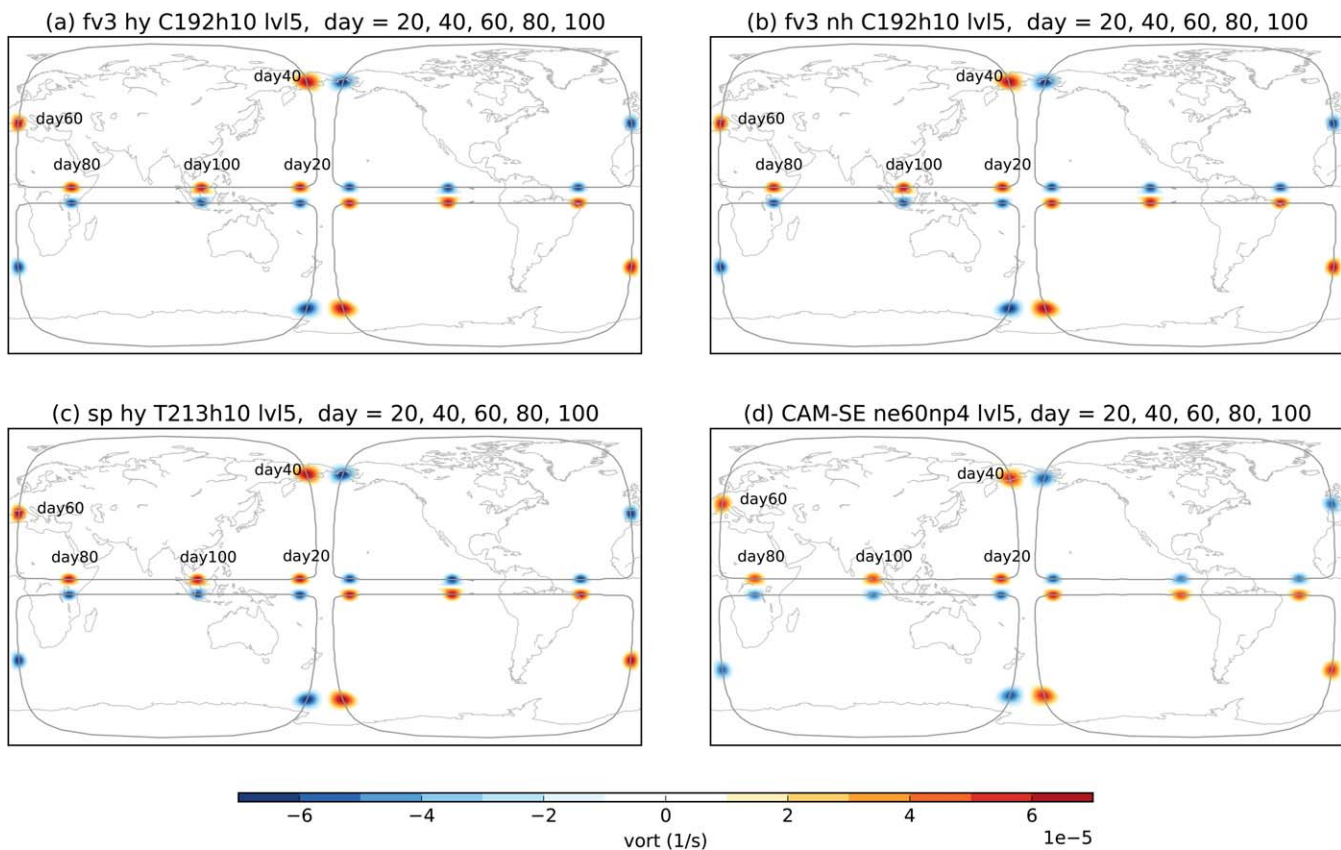


Figure 6. Three-dimensional simulations at 50 km resolution depicting vorticity in the lowest of the five model levels. (a) Hydrostatic FV³ C192, (b) nonhydrostatic FV³ C192, (c) hydrostatic spectral T213, and (d) CAM-SE ne60np4.

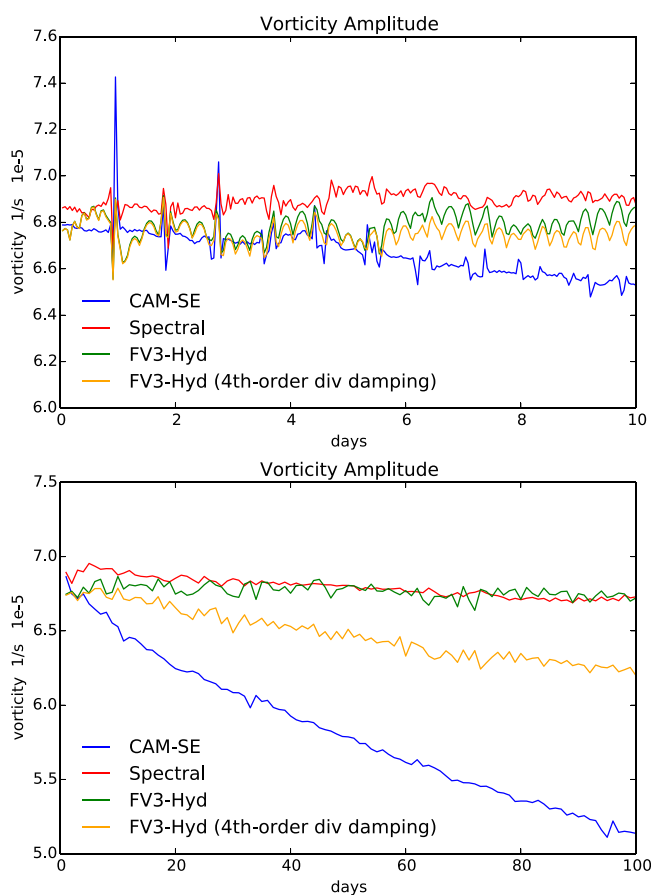


Figure 7. Domain-maximum vorticity of 50 km resolution equivalent hydrostatic simulations in each dynamical core. (top) Hourly maxima for the first 10 days of the simulation. (lower) Daily maxima for the entire 100 day integration time of each simulation. Note that the CAM-SE uses a fourth-order (less scale-selective) hyperdiffusion. The nonhydrostatic FV³ solution’s vorticity maximum is identical to that of the hydrostatic solver and is not shown here.

averaged speed of 5 m/s, similar to that of the Madden-Julian Oscillation. After the collision, the modons exchange vortices and then propagate poleward, colliding and exchanging vortices again at day 70 at the equator. By day 100, the modons have passed through their initial positions and have begun a new cycle. A perfect model with no diffusion (implicit or explicit) or phase errors should allow the modon pairs to continue this cycle indefinitely; however, a realistic model should still be expected to finish at least one cycle while maintaining some resemblance to the original modon pair.

How does the solution change with increased resolution? A 25 km or C384 resolution shallow-water FV³ simulation is shown in Figure 4b, with the solutions every 20 days superposed onto one panel. Despite the doubled resolution the positions of the modons are nearly identical to that of the 50 km FV³ simulation in Figure 3, indicating that the 50 km solution is converged.

How does the solution depend on the specific horizontal discretization? Two simulations using the shallow-water GFDL spectral core, at T213 (Figure 4c) and T511 (Figure 4d) truncations, were performed. Both the trajectories and the amplitude of the modons from the spectral core are very similar to FV³. There is a small shift eastward in the day-100 location of the eastward modon in the T511 simulation compared to the T213 simulation, which is larger than the very minor shift in the C192 and C384 FV³ solutions.

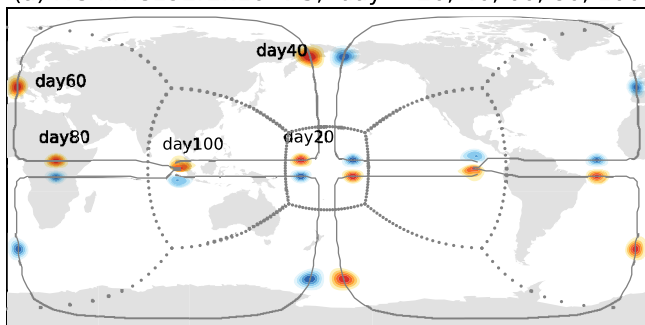
The modon configuration is symmetric across the cubed-sphere grid used by FV³ and CAM-SE, as the modons are propagating along grid lines. How would the results change if the grid were rotated? Figure 5 shows the results from a simulation in which the cubed sphere is rotated by 45 degrees, so that the modons pass through the corners and obliquely through at least two of the faces. The results are still nearly identical—judged by the trajectories and the final placement of the modons—to that for the unrotated grid—demonstrating the robustness of the FV³ discretization.

3.3. Hydrostatic and Nonhydrostatic Solutions

The three-dimensional hydrostatic simulations with all three cores are very similar. Figure 6a shows the FV³ hydrostatic C192 resolution result at the surface. The FV³ hydrostatic simulation is almost the same as the shallow-water simulation, as are the nonhydrostatic FV³ and the hydrostatic GFDL spectral model (Figures 4b and 4c, respectively). CAM-SE with a ne60np4 resolution (equivalent to C192 in FV³) shows greater diffusion (Figure 6d) than the other cores even when reducing the fourth-order diffusion coefficient by a factor of five from the default value. This reduction in the diffusion was necessary to maintain the modon structure and to prevent excessive slowdown of the propagation of the modon. Further reduction of this coefficient does not further reduce the dissipation of the modon. As noted earlier no sponge layer is applied in any of the cores.

It is also interesting to compare the relative propagation speeds of the modon by considering their relative positions on day 100. From Figure 6, we can see that the FV³ hydrostatic simulation is the fastest, the GFDL spectral model slightly slower, and CAM-SE the slowest; the difference between the locations, however, is less than about 1,000 km, implying a difference in propagation speeds of about 0.1 m s⁻¹. The slight difference in speeds may reveal something about the characteristics of vorticity advection in each model. We do wish to stress that, in the absence of an analytic solution, we have no way of knowing which propagation speed is “correct.” The goal of the test is not to produce the fastest-propagating modon, and a faster propagation speed should not be interpreted as a better result. Further discussion of propagation speed lies beyond the scope of this paper.

(a) fv3 nh C192r2h10 lvl5, day = 20, 40, 60, 80, 100



(b) fv3 nh C192r3h10 lvl5, day = 20, 40, 60, 80, 100

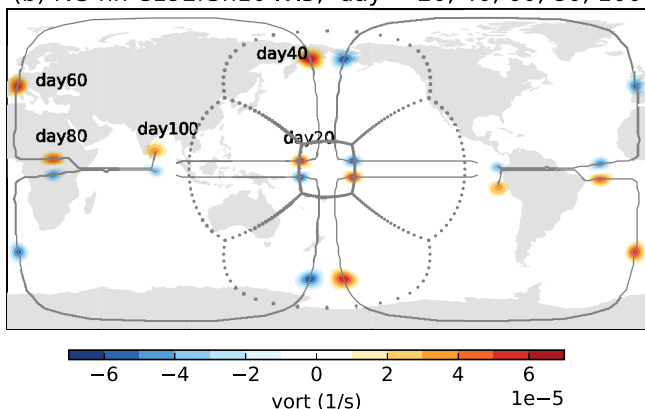


Figure 8. The vorticity of the lower-most full-model level closest to the ground as in Figure 6 but with (a) C192r2 and (b) C192r3 nonuniform, nonhydrostatic FV³. The gray dots are the stretched-cubed-sphere tile interfaces. Note the “flower” formed by the grid outlines.

which gradually enhances the resolution on one grid face while degrading the opposite face, with smooth transition on the four other faces of the cube. The resulting deformed grid resembles a flower with four petals (as depicted in Figure 8), the center of which is the target high-resolution region. More details are given in Harris et al. (2016).

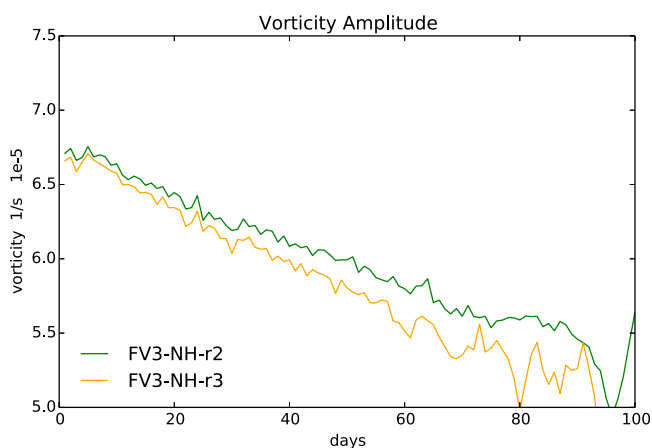


Figure 9. As in Figure 7 but for C192r2 and C192r3 nonuniform, nonhydrostatic FV³.

The time series of domain-maximum vorticity for each hydrostatic simulation (Figure 7) shows that the modon amplitude in CAM-SE is decaying more rapidly than in the spectral core and FV³. Interestingly, the spectral core appears to show less oscillation in time than FV³. The vorticity maximum of the nonhydrostatic FV³ solution is virtually identical to that of the hydrostatic FV³ solution, indicating that the nonhydrostatic component does not fundamentally alter the diffusive or advective behavior of the solver and that both the nonhydrostatic and hydrostatic solvers behave correctly in the hydrostatic limit.

Why is CAM-SE more diffusive than FV³ and the spectral core? We have found that this depends at least in part on the scale selectiveness of the diffusion used. In FV³, we typically use a sixth-order divergence damping (except in stretched-grid simulations in which fourth-order dissipation is used), whereas in CAM-SE, a less scale-selective fourth-order hyperdiffusion is used. For well-resolved disturbances, we would expect that the cumulative diffusion of the solution when using fourth-order diffusion would be greater. To test this, a C192 hydrostatic FV³ simulation was performed with fourth-order damping; to compensate for the reduced scale-selectivity, the diffusion coefficient was decreased from 0.15 to 0.12. The rate at which the vorticity was dissipated was then more similar (albeit slower) compared to that of CAM-SE (Figure 7), partially validating our hypothesis. There is a minor westward shift of the location of the modon at day 100 in the fourth-order dissipation FV³ simulation (not shown), but it is not shifted as far west as in the CAM-SE simulation.

3.4. Nonhydrostatic Solutions on Nonuniform Grids

Nonuniform grids allow the dynamical core to locally improve the simulation in a chosen focus region without the expense of a globally uniform high resolution simulation. However, a nonuniform grid may distort propagating features and/or the global circulation. Here we test the ability of FV³ to maintain the modon pairs as they pass through a refined region. The cubed-sphere grid is stretched using the Schmidt (1977) transformation,

which gradually enhances the resolution on one grid face while degrading the opposite face, with smooth transition on the four other faces of the cube. The resulting deformed grid resembles a flower with four petals (as depicted in Figure 8), the center of which is the target high-resolution region. More details are given in Harris et al. (2016).

In this test, the modons enter the high resolution area centered at $(\pi, 0)$ through the east and west sides, respectively; collide, exchanging vortices; and exit the high-resolution region toward the poles in opposing directions. Two nonuniform grids are used: the first, called C192r2, is a C192 base grid deformed by a stretch factor of 2, so that the grid-cell-width varies from about 25 km at highest resolution (equivalent to the C384 grid shown previously) to 100 km at coarsest resolution. The second nonuniform grid, called C192r3, is a C192 base grid deformed by a stretch factor of 3, with grid-cell widths varying from 17 to 150 km. For stretched-grid simulations using FV³, a less scale-selective fourth-order damping was used due to the changing resolution, again with the diffusion coefficient reduced to 0.12.

Our results demonstrate that both nonuniform grids (Figure 8) successfully resolved the collision process of the two modons. The symmetric motion of the modons is maintained for at least 80 days with C192r2 grid (Figure 8a) and 60 days with the more aggressively stretched C192r3 grid (Figure 8b). The issues with the C192r3 configuration may in part be due to the coarse

150 km grid-cell width in the degraded-resolution region, which may not be sufficient to resolve the 500 km wide vortices. In both stretched-grid simulations, the amplitude of the modons decays roughly linearly (Figure 9) until the modons break; the decay rate is faster than in the uniform-resolution fourth-order damping simulation (Figure 7). The decay rate is slower and the modon lasts longer on the C192r2 grid, showing that more aggressive stretching can cause the modon to be diffused more quickly.

4. Conclusions

We presented an easy-to-implement modon test case that demonstrates readily interpreted behavior relative to that of counter-rotating vortices, and gives a challenging test of the core's ability to maintain strongly nonlinear rotational flow without spurious vorticity generation. To simplify this test case and to allow the modons to collide and exchange pairs, there is no planetary rotation, and the flow is initially barotropic. A further simplification of the test specification is that we do not specify a fully balanced initial condition, but allow the model to self-adjust to cyclostrophic balance, thereby creating a stronger test of the dynamical core. Formulations are given for shallow-water, stratified hydrostatic, and stratified nonhydrostatic solvers.

We have shown results from a variety of solvers, for both shallow-water and stratified flow, using three different horizontal discretizations, and also results using the nonhydrostatic option of the GFDL FV³ core. The simulated modons behave similarly between all the solvers, which all maintain the modons for 100 days and have similar positions on any particular day, although some difference in propagation and amplitude between cores and due to the explicit diffusion are apparent. Neither the radiated gravity waves created by the initial adjustment nor the depth of the flow nor the choice of equation set (shallow water, hydrostatic, or nonhydrostatic) affect the propagation or diffusion of the modons in our tests.

Vertical motion has little to no effect on this test. The three different forms of the FV³ solver—shallow-water, hydrostatic, and nonhydrostatic—show nearly identical solutions. We did find that while the motion of the modon was similar between the solvers, the variability, and secular decay of the modon's amplitude was dependent upon the amount of dissipation, whether implicit or explicit, in the horizontal solver. We also performed the modon test using FV³'s stretched-grid option. While the modon passed through the refined region without significant distortion, the modon was diffused and eventually began to break after passing through the degraded-resolution region on the opposing side of the domain.

We have shown that the test design and evaluation method is sufficiently robust to be used with a wide range of solver types, numerical methods, diffusion types, and grid configurations, and that the test does not require any particular form of these. We encourage model developers to use this test as a means of exploring the effects of different design and configuration choices of their dynamical cores, as a development and debugging tool. Our only recommendation for presenting results from a core is that modelers use the same type, and same order of magnitude, of diffusion as would be used in a full-physics weather or climate simulation (excluding the top sponge layer), to ensure that the results are representative of real-world model use.

Global models with a height-based vertical coordinate (and with a rigid lid) tend to apply additional filters to suppress the external mode (Jablonowski & Williamson, 2011, section 13.4.4). If for stability reasons, the strength of such "external mode" filter is very strong, the model could become highly dissipative under weak wind shear conditions (more barotropic) when the real-world cyclogenesis is most favorable. Models with a split-explicit time integration scheme (large time step for advection and small time step for fast waves) may generate spurious vorticity (due to noncancellation of the pressure gradient terms with the "curl" of the momentum equation), and might have more difficulties for this vorticity-centric test. Test like the one presented here are therefore useful for the validation of numerical algorithms that may have the aforementioned issues that are difficult to diagnose when running with full-physics for weather predictions or climate simulations.

References

- Batchelor, G. (1967). *An introduction to fluid dynamics* (635 pp.). Cambridge, UK: Cambridge University Press.
- Butchart, N., Haines, K., & Marshall, J. C. (1989). A theoretical and diagnostic study of solitary waves and atmospheric blocking. *Journal of the Atmospheric Sciences*, 46(13), 2063–2078.
- Chen, X., Andronova, N., Van Leer, B., Penner, J. E., Boyd, J. P., Jablonowski, C., & Lin, S.-J. (2013). A control-volume model of the compressible Euler equations with a vertical Lagrangian coordinate. *Monthly Weather Review*, 141(7), 2526–2544.

Acknowledgments

We thank Mark Taylor from Sandia National Laboratory for helping with the CAM-SE configurations, and Alistair Adcroft and Steve Garner for useful internal reviews. We also thank two anonymous reviewers for their reviews. Yao and Chen's participation was funded through NOAA's Sandy Supplemental Project. All materials used in this work are stored through GFDL's Archiving Systems at the location "/archive/Xi.Chen/PAPERS/2017.JAMES.Modon/data/" and can be obtained by contacting GFDL or the corresponding author.

- Colella, P., & Woodward, P. R. (1984). The Piecewise Parabolic Method (PPM) for gas-dynamical simulations. *Journal of Computational Physics*, 54(1), 174–201.
- Flierl, G. R. (1979). A simple model for the structure of warm and cold core rings. *Journal of Geophysical Research*, 84(C2), 781–785.
- Flierl, G. R. (1987). Isolated eddy models in geophysics. *Annual Review of Fluid Mechanics*, 19(1), 493–530.
- Harris, L. M., & Lin, S.-J. (2013). A two-way nested global-regional dynamical core on the cubed-sphere grid. *Monthly Weather Review*, 141(1), 283–306.
- Harris, L. M., Lin, S.-J., & Tu, C. (2016). High-resolution climate simulations using GFDL HiRAM with a stretched global grid. *Journal of Climate*, 29(11), 4293–4314.
- Held, I. M., & Suarez, M. J. (1994). A proposal for the intercomparison of the dynamical cores of atmospheric general circulation models. *Bulletin of the American Meteorological Society*, 75(10), 1825–1830.
- Ingersoll, A. P. (1973). Jupiters great red spot: A free atmospheric vortex? *Science*, 182(4119), 1346–1348.
- Jablonowski, C., & Williamson, D. L. (2006). A baroclinic instability test case for atmospheric model dynamical cores. *Quarterly Journal of the Royal Meteorological Society*, 132(621C), 2943–2975.
- Jablonowski, C., & Williamson, D. L. (2011). The pros and cons of diffusion, filters and fixers in atmospheric general circulation models. In P. H. Lauritzen, C. Jablonowski, M. A. Taylor, & R. D. Nair (Eds.), *Numerical techniques for global atmospheric models, Lecture notes in computational science and engineering* (pp. 381–493). Berlin: Springer.
- Lamb, H. (1932). *Hydrodynamics*. Cambridge, UK: Cambridge University Press.
- Lin, S.-J. (1997). A finite-volume integration method for computing pressure gradient force in general vertical coordinates. *Quarterly Journal of the Royal Meteorological Society*, 123(542), 1749–1762.
- Lin, S.-J. (2004). A “Vertically Lagrangian” finite-volume dynamical core for global models. *Monthly Weather Review*, 132(10), 2293–2307.
- Lin, S.-J., & Rood, R. B. (1997). An explicit flux-form semi-Lagrangian shallow-water model on the sphere. *Quarterly Journal of the Royal Meteorological Society*, 123(544), 2477–2498.
- McWilliams, J. C. (1980). An application of equivalent modons to atmospheric blocking. *Dynamics of Atmospheres and Oceans*, 5(1), 43–66.
- Muraki, D. J., & Snyder, C. (2007). Vortex dipoles for surface quasigeostrophic models. *Journal of the Atmospheric Sciences*, 64(8), 2961–2967.
- Putman, W. M., & Lin, S.-J. (2007). Finite-volume transport on various cubed-sphere grids. *Journal of Computational Physics*, 227(1), 55–78.
- Reed, K. A., & Jablonowski, C. (2012). Idealized tropical cyclone simulations of intermediate complexity: A test case for AGCMs. *Journal of Advances in Modeling Earth Systems*, 4, M04001. <https://doi.org/10.1029/2011MS000099>
- Reed, K. A., Medeiros, B., Bacmeister, J. T., & Lauritzen, P. H. (2015). Global radiative-convective equilibrium in the community atmosphere model, version 5. *Journal of the Atmospheric Sciences*, 72(5), 2183–2197.
- Rex, D. F. (1950). Blocking action in the middle troposphere and its effect upon regional climate. *Tellus*, 2(4), 275–301.
- Robert, A. (1993). Bubble convection experiments with a semi-implicit formulation of the Euler equations. *Journal of the Atmospheric Sciences*, 50(13), 1865–1873.
- Schär, C., Leuenberger, D., Fuhrer, O., Lüthi, D., & Girard, C. (2002). A new terrain-following vertical coordinate formulation for atmospheric prediction models. *Monthly Weather Review*, 130(10), 2459–2480.
- Schmidt, F. (1977). Variable fine mesh in spectral global models. *Beitraege zur Physik der Atmosphaere*, 50, 211–217.
- Scott, R. K., Harris, L. M., & Polvani, L. M. (2016). A test case for the inviscid shallow-water equations on the sphere. *Quarterly Journal of the Royal Meteorological Society*, 142(694), 488–495.
- Scott, R. K., & Polvani, L. M. (2007). Forced-dissipative shallow-water turbulence on the sphere and the atmospheric circulation of the giant planets. *Journal of the Atmospheric Sciences*, 64(9), 3158–3176.
- Snyder, C., Muraki, D. J., Plougonven, R., & Zhang, F. (2007). Inertia-gravity waves generated within a dipole vortex. *Journal of the Atmospheric Sciences*, 64(12), 4417–4431.
- Straka, J. M., Wilhelmson, R. B., Wicker, L. J., Anderson, J. R., & Droegemeier, K. K. (1993). Numerical solutions of a non-linear density current: A benchmark solution and comparisons. *International Journal for Numerical Methods in Fluids*, 17(1), 1–22.
- Taylor, M. A., & Fournier, A. (2010). A compatible and conservative spectral element method on unstructured grids. *Journal of Computational Physics*, 229(17), 5879–5895.
- Tribbia, J. J. (1984). Modons in spherical geometry. *Geophysical & Astrophysical Fluid Dynamics*, 30(1–2), 131–168.
- Ullrich, P. A., Jablonowski, C., Kent, J., Lauritzen, P. H., Nair, R. D., & Taylor, M. A. (2012). *Dynamical core model intercomparison project (DCMIP) test case document*. Boulder, CO. Retrieved from https://site_media/docs/DCMIP-TestCaseDocument_v1.7.pdf
- Vanneste, J. (2013). Balance and spontaneous wave generation in geophysical flows. *Annual Review of Fluid Mechanics*, 45(1), 147–172.
- Williamson, D. L., Drake, J. B., Hack, J. J., Jakob, R., & Swarztrauber, P. N. (1992). A standard test set for numerical approximations to the shallow water equations in spherical geometry. *Journal of Computational Physics*, 102(1), 211–224.
- Zhao, M., Held, I. M., & Lin, S.-J. (2012). Some counterintuitive dependences of tropical cyclone frequency on parameters in a GCM. *Journal of the Atmospheric Sciences*, 69(7), 2272–2283.